

# MATHEMATICAL MODELING OF THE MELT FLOW IN THE CONE-RING CHANNEL OF THE EXTRUDER MATRIX

**Abdymanap Ospanov**

Doctor of Technical Sciences, Professor\*

**Aigul Timurbekova**

Corresponding author

Candidate of Technical Sciences, Professor\*

E-mail: timurbekova\_aigul@mail.ru

**Dulat Zhalelov**

Master of Technical Sciences, Senior Lecturer\*

\*Department of Technology and Food Safety

Kazakh National Agrarian Research University

Abay ave., 8, Almaty,

Republic of Kazakhstan, 050010

*The peculiarity of the work is to develop a mathematical model of the melt flow in the cone-annular channel of the extruder die, which will allow you to choose the optimal geometric shape of the annular channel, as well as the angular rotation speed of the extruder screw. The object of the study is the cone-ring channel of the extruder matrix.*

*To solve the three-dimensional problem of turbulent and laminar unsteady motion, the FlowVision software package was used, which allows solving partial differential equations using the finite volume method. The correct choice of the geometric shape of the annular gap made it possible to change the molecular structure of the product by creating a maximum pressure value. The optimally selected angular rotation speed of the extruder screw made it possible to carry out deep melting of the product due to the conversion of the mechanical energy of the screw into thermal energy.*

*In the process of designing the forming of the cone-ring channel, the three volumes of the changing geometry of the stamp were selected, at the borders of the transition of which extreme points were observed. Deviations between the analyzed and experimental values of velocity and pressure were found in the limits of 9–12% and 17–22%, respectively.*

*Based on the analysis of the obtained results of modeling, the optimal geometric shape of the annular gap and the recommended angular rotation speed of the extruder screw were revealed.*

*The mathematical model proposed formed the basis of the developed design of the six-zone extruder. In the extruder, the geometric characteristics of the screw (variable pitch of the turns) were substantiated and selected, which provide the maximum effect of dissipation, i.e. autogenous mode of operation*

*Keywords: mathematical model, FlowVision, combined feed, cone-ring channel, extruder matrix*

Received date 14.11.2023

Accepted date 30.01.2024

Published date 28.02.2024

**How to Cite:** Ospanov, A., Timurbekova, A., Zhalelov, D. (2024). Mathematical modeling of the melt flow in the cone-ring channel of the extruder matrix. *Eastern-European Journal of Enterprise Technologies*, 1 (7 (127)), 83–98.

doi: <https://doi.org/10.15587/1729-4061.2024.290692>

## 1. Introduction

Optimal design of extrusion equipment, achieved by improving the theory and methods of its calculation, will ensure the production of products of the required quality [1, 2]. Extrusion processes are subject to various substantial challenges due to the need in variety, efficiency, and productivity [3]. Mathematical modeling and simulation of conjugate flow, deformation, heat and mass transfer, as well as the rate of reactions occurring in a twin-screw extruder, make it possible to optimize the process parameters [4, 5]. For example, by increasing the screw speed from 8 to 15 rpm, you can increase productivity up to 3 times [6].

Extrusion is a special method of processing raw materials, in which the mixed powder is subjected to mechanical action from the screw part of the extruder. The process takes place under the influence of high temperatures (about 150 °C) and pressure. The crushed mass heated under high pressure is then placed under low pressure. As a result of such a rapid change, a so-called “explosion” occurs, the final product increases in volume and acquires a porous structure. Extrusion is distinguished not only by its versatility, productivity and efficiency, but also by its low cost and low amount of waste.

Extrusion technology is a high-temperature, short-term continuous food processing technology (HTST) combining mechanical and thermal energy for starch gelatinization,

protein denaturation and reorganization of food materials to form new textures [7].

Variations in extrusion parameters, such as the composition of raw materials, the configuration of the die, the feed rate and the processing temperature, especially strongly affect the quality of the final product. Therefore, it is very important to optimize the production parameters correctly and efficiently during the product extrusion process [7]. The Response Surface Methodology (RSM) and central composite design (CCD) are ideal tools for process optimization [7].

The extrusion process consists of several stages: loading, compression, homogenization (plasticization), pressure stabilization zone. However, some researchers, in order to describe most accurately the behavior of the material in the working chamber of the extruder, distinguish more technological zones (for example, mixing zone, pre-matrix zone or dosing zone, etc.), which is probably more logical and appropriate for further in-depth study of the extrusion process. In addition, the housing of the working chamber of the extruder under study is made detachable and consists of six zones, five of which provide steam input into the double-track housing to ensure a polytropic mode of operation, which corresponds to the most advanced world technologies.

This makes it possible to provide maintenance and optimal temperature control along the entire length of the working body of the extruder. Thus, mathematical modeling

of the melt flow in the cone and annular channels of the extruder matrix is a fairly urgent task.

---

## 2. Literature review and problem statement

---

A significant contribution to the development of mathematical models and methods of calculating extruders was made by [7]. However, the determination of the velocity and pressure fields that determine the quality of the finished product and the performance of the extrusion plant remains poorly understood.

In [8], the process of extrusion of amaranth grain for animal feed was researched at the following parameters: temperature 110–158 °C, screw rotation speed (40–52 s<sup>-1</sup>) and moisture content in the feed (11–16 %). The study used multiple response criteria using the response surface methodology and desirability function analysis, and the variable responses were protein digestibility, sensory acceptability, water absorption index, water solubility index, bulk density and viscosity. Optimal extrusion parameters were identified: temperature 150 °C, screw rotation speed 50 s<sup>-1</sup> and moisture content in the raw material 14.41 %. This made it possible to achieve the digestion of 81.87 % protein, a water solubility index of 0.55 and a sensory acceptability score of 6.69 with a desirability of 71 %. However, the problem with making is the long preparing time, the use of more resources and the high viscosity. Therefore, food processing technologies that increase the nutritional value of the combined feed are recommended.

In [9, 10], the effectiveness of the extrusion process on the quality indicators of combined feed with the extruded waste of oilseeds containing a sufficient amount of protein and raw fat, which can be used in animal feeding diets to increase milk productivity, was investigated. Using mathematical methods of planning a multifactorial experiment, a mathematical model of the process of extrusion of feed raw materials has been developed. Based on the obtained model, the recommended modes of extrusion of feed raw materials from post-harvest waste are determined.

It was found that there is a directly proportional relationship between the viscosity of the final product and the content of moisture, lipids and simple sugars in it, and an inversely proportional dependence of viscosity on the temperature of the extrusion process and the rotation speed of the screw.

The solution to this problem was obtained by planning multifactorial experiments, statistical processing of experimental data and search engine optimization.

An analytical solution of a two-dimensional non-isothermal mathematical model describing the change in the velocity profile of a cylindrical extrusion head is presented [11]. The mathematical model was constructed from the incompressibility equation, the equations of motion, the energy equation and the rheological equation [12]. This model depicted a non-isothermal flow of rheological fluid moving through a cylindrical extrusion head. Computer testing was carried out to verify the solutions obtained and compare them with the actual extrusion process. The difference between the calculated and experimental data was below 14 %. The results allow us to conclude that the numerical results are consistent with experimental data, therefore, a composite model can be used in the design of an extrusion head for single-screw extruders.

In [13], methods of mathematical analysis and data processing in the Math CAD (Voronezh State University

of Engineering Technologies) software environment were used and graphical dependences of the power and energy parameters of the oil-containing raw material extrusion process using a twin-screw extruder were obtained. With an increase in the density of the oil-containing raw materials in the extruder by 40.5 %, the pressure force increases by 41 %, that is, there is an almost proportional relationship between the pressure force and the density of the processed raw materials. With an increase in the angular velocity of the screw more than 8 s<sup>-1</sup>, the pressure force during the study increases sharply. With an increase in the density of raw materials, it is crushed before extrusion by 40 %, the energy consumption for the grinding process increases by 2.8 times for the recommended operating mode. Energy losses during pressing of completely crushed raw materials are reduced by 2.52 times.

However, effective mathematical modeling of twin screw extruders has long been limited to the development of geometric parameters and the justification of processing modes based on practical experience and experimental data, due to the rather complex design of the executive bodies.

As we can see, mathematical models of melt formation from solid bulk product particles in the homogenization zone of the extruder were previously investigated.

The authors do not consider the process of melting and homogenization of the bulk mixture of the initial product, as a result of which, due to the dissipation effect, the mechanical energy of the working bodies of the machine is converted into thermal energy, i.e. the product, compacting, warms up due to the friction forces of particles on the surface of rotating working bodies and shear deformations in the product itself and passes from the bulk solid phase to liquid (in the form of a gel-like, viscous melt). We draw attention to the fact that the next stage of processing of an already formed melt is considered, namely, the three-dimensional problem of turbulent and laminar unsteady melt flow in the cone-ring channel of the extruder matrix. In this case, the resulting melt is moved by a screw in the cone-ring channel of the extruder matrix and is pressed out through its holes under pressure.

Mathematical modeling of the movement of the technological medium at individual stages of raw material processing allows us to determine the analytical dependences of the power and energy parameters of the system and carry out their effective technical and economic assessment.

---

## 3. The aim and objectives of the study

---

The aim of the study is mathematical modeling of the melt flow in the cone and annular channels of the extruder die, which will allow you to choose the optimal geometry of the annular channel and the angular rotation speed of the extruder screw.

To achieve the aim, the following objectives were set:

- to denote the optimal geometric shape of the annular gap;
- to determine the recommended angular rotation speed of the extruder screw.

---

## 4. Materials and methods

---

The object of the study is the cone-ring channel of the extruder matrix.

The main hypothesis of the research is to develop a mathematical model of the melt flow in the cone-annular channel

of the extruder die, which will allow you to choose the optimal geometric shape of the annular channel, as well as the angular rotation speed of the extruder screw.

The main assumptions of the work: at the boundary of the calculation area, the Boolean subtraction of the volume of cells that did not fall into the calculation area from a rectangular element is used, as a result of which the required calculation area is formed from the remaining cell volumes. The FlowVision software package automatically created a computational grid with the possibility of an additional increase in the number of cells in areas with a complex configuration.

To solve the 3D problem of unsteady motion of turbulent and laminar flows, the FlowVision software package was used, which can solve partial differential equations using the finite volume method.

Assuming that each cell represents a finite volume, the differential equations being solved are approximated on a computational grid, where the rate of change of physical quantities is balanced by quantities passing through the edge of the cell. The streaming representation of the computing network is cartesian with local adaptation of the original grid in accordance with the specified partitioning criteria.

Based on a single-screw extruder, three forming channels of the matrix were designed to select the most optimal geometric parameters of the die, which affect the depth of physico-chemical transformations occurring in the structure of the finished product (Fig. 1).

The most suitable graphic editor for three-dimensional design is COMPASS-3D V18, and the designed three-di-

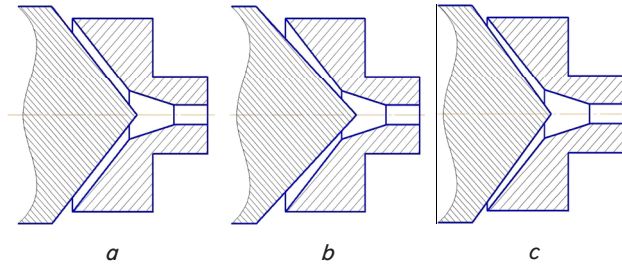


Fig. 1. Forming channels of the extruder matrix: *a* – parallel; *b* – narrowing; *c* – expanding

mensional model of the forming cone-ring channel was imported into the FlowVision software package.

## 5. Results and analysis of mathematical modeling and optimization of melt flow

### 5.1. Designation of the optimal geometric shape of the annular gap

The next step in modeling the melt flow in a cone-ring channel is the choice of a mathematical model and solvable equations that are included in the selected model. Based on the results of the conducted research in this area, it was found that the mode of movement of the extrudate is laminar.

In the FlowVision software package, the laminar flow mode was calculated using the “incompressible fluid” model, disabling the equations for turbulent transfer functions from the calculation.

We introduce the following assumptions:

- the process is isothermal due to the fact that the product melt in the cone-ring channel overcomes the distance

from the inlet to the outlet of the channel in such a short period and the extruder body is equipped with a system to maintain a constant temperature;

- we neglect the mass transfer equation since the melt entering the cone-ring channel has a homogeneous structure.

The main design dimensions of the extruder screw are as follows: screw diameter – 160 mm; variable pitch sizes of the screw turns: 120 (at a length of 360 mm); 90 (at a length of 360 mm); 60 (at a length of 240 mm, two-way, step between turns 30); 60 (at a length of 120 mm); 90 (at a length of 360 mm, three-way, step between turns 30).

For the numerical solution of differential equations describing the flow of liquids and gases whose thermophysical properties vary in a wide range, the finite volume method is used in channels with a complex geometric shape in the software shell.

The selected model includes the following equations:

- Navier-Stokes:

$$\frac{\partial v_x}{\partial \tau} + \frac{\partial (v_x^2)}{\partial x} + \frac{\partial (v_x v_y)}{\partial y} + \frac{\partial (v_x v_z)}{\partial z} = -\frac{\partial P}{\partial x} + \frac{1}{Re} \nabla^2 v_x, \tag{1}$$

$$\frac{\partial v_x}{\partial \tau} + \frac{\partial v_y}{\partial \tau} + \frac{\partial (v_x v_y)}{\partial x} + \frac{\partial (v_y^2)}{\partial y} + \frac{\partial (v_x v_y)}{\partial z} = -\frac{\partial P}{\partial y} + \frac{1}{Re} \nabla^2 v_y, \tag{2}$$

$$\frac{\partial v_x}{\partial \tau} + \frac{\partial (v_x v_z)}{\partial x} + \frac{\partial (v_y v_z)}{\partial y} + \frac{\partial (v_z^2)}{\partial z} = -\frac{\partial P}{\partial z} + \frac{1}{Re} \nabla^2 v_z, \tag{3}$$

where:

$$\nabla^2 v_x = \frac{\partial^2 v_x}{\partial x^2} + \frac{\partial^2 v_x}{\partial y^2} + \frac{\partial^2 v_x}{\partial z^2},$$

$$\nabla^2 v_y = \frac{\partial^2 v_y}{\partial x^2} + \frac{\partial^2 v_y}{\partial y^2} + \frac{\partial^2 v_y}{\partial z^2},$$

$$\nabla^2 v_z = \frac{\partial^2 v_z}{\partial x^2} + \frac{\partial^2 v_z}{\partial y^2} + \frac{\partial^2 v_z}{\partial z^2}.$$

The continuity equation:

$$D \equiv \nabla \cdot V \equiv \frac{\partial v_x}{\partial x} + \frac{\partial v_y}{\partial y} + \frac{\partial v_z}{\partial z} = 0. \tag{4}$$

When solving equations (1)–(4), the following boundary conditions were taken into account: the wall formed by the inner surface of the die, the cone of the rotating screw, the entrance to the cone-ring channel and the exit from it.

In the FlowVision software package, to set boundary conditions, the imported 3D model undergoes geometry rearrangement with the assignment of the resulting groups to the selected boundary conditions.

a) The wall formed by the inner surface of the die (Fig. 2).

Type of the specified boundary: wall.

Type of the specified boundary condition: wall.

A condition for sticking is set at the boundary of the area:

$$v|_w = 0. \tag{5}$$

b) The cone of the rotating screw (Fig. 3).

Type of the specified boundary: wall.

Type of the specified boundary condition: tangential twist.

This boundary condition defines a velocity vector having a tangent component  $v_k$  to the boundary surface (there is no normal component  $v_n=0$ ).

The direction of rotation is determined by the rule of the gimlet and the sign of the degree of twist) –  $-\omega > 0$  “forward” rotation;  $\omega < 0$  – “reverse” rotation.

The direction of the tangent component of the velocity is determined by the rule of the gimlet applied to the vector. The actually calculated boundary is represented by flat facets. Therefore, the speed determined by the rule of the gimlet may have a component normal to the facet. In calculations, this component is assumed to be equal to zero. The resulting error can be reduced by improving the quality of the facet representation of the surface. We set the rotation speed of the extruder screw to 20, 30, 40 and 50 rad/s.

c) Entrance to the cone-ring channel.

Type of the specified boundary: input/output.

Type of the specified boundary condition: normal speed.

The normal component of the velocity vector is set at the boundary of the region  $v_{nw}$ :

$$v|_n = v_{nw}. \tag{6}$$

If  $v_{nw} > 0$ , then the area highlighted in Fig. 3, *a* is assigned the flow direction value «input». If  $v_{nw} < 0$ , then the area in Fig. 3, *c* is «outlet». If the resulting value has a negative value  $v_{nw}$  as a result of the calculation, then it changes according to the following rule: «How much mass has flowed in – so much mass has flowed out», i.e. the mass balance is observed:

$$v_w^{out} = -(\sum v_w^{in} S^{in}) / (\sum S^{out}), \tag{7}$$

where  $S^{in}$  is the area of the boundary surface “entrance” – the area of the boundary surface «outlet».

d) Exit from the cone-ring channel (Fig. 3).

Type of the specified boundary: free outlet.

Type of the specified boundary condition: zero pressure/outlet.

The speed at the boundary of the calculated area is set according to the following rule:

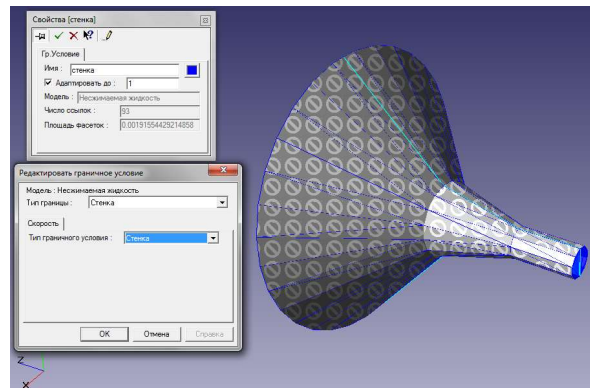
- in the calculation cell adjacent to the boundary, the direction of the velocity vector is determined;
- if the velocity vector is directed inside the calculated area, then the normal component of the velocity is reset to zero;
- if the velocity vector is directed from the computational domain, then the normal derivatives of the components of the velocity vector equal to zero are established:

$$p|_w = 0, \tag{8}$$

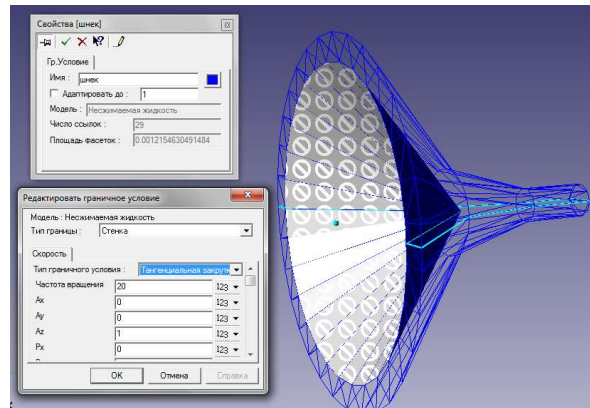
$$(v, n) > 0, \quad v|_w = v_{tw}, \tag{9}$$

$$(v, n) < 0, \quad \Delta(v_i, n)|_w = 0, \tag{10}$$

here  $n$  is normal to the boundary,  $v_{tw}$  is the tangential component of the velocity at the boundary.

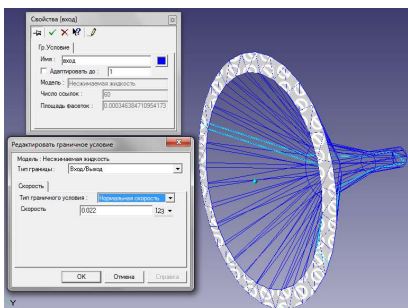


*a*

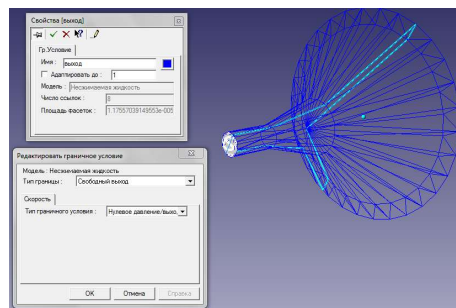


*b*

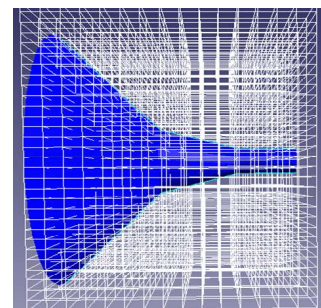
Fig. 2. Boundary condition: *a* – wall; *b* – rotating screw cone



*a*



*b*



*c*

Fig. 3. Boundary condition: *a* – entrance to the cone-ring channel; *b* – exit from the cone-ring channel; *c* – adapted calculation grid

The following melt properties were introduced into the mathematical model as calculated physical parameters: density 1,120 kg/m<sup>3</sup>, 1,170 kg/m<sup>3</sup> and 1,210 kg/m<sup>3</sup>.

The space in the ranges of which we seek a solution of the differential equations is divided into a finite number of elements, thus creating a computational grid that allows you to accurately and easily describe complex geometries (Fig. 3, c).

The initial adaptation of the computational grid is produced by the boundary condition with the choice of criteria of split: wall formed by the inner surface of the die, cone rotating the screw, the entrance to the conical-ring channel and the output of it.

### 5. 2. Determination of the recommended angular rotation speed of the extruder screw

According to its structure, the computational grid is rectangular cells that are evenly distributed over the entire section of the calculated variant, but when approaching the periphery of the calculated area, the parallelepipeds are rearranged, with the formation of polyhedra that completely repeat the calculated area. Then a program is launched that generates a calculated grid.

The next step was to set the parameters of the numerical simulation method. The FlowVision program uses the finite volume method for the numerical solution of convective-diffusion transport equations, written in general form as:

$$\frac{\partial f}{\partial t} + \nabla(Vf) = \nabla(DVf) + Q, \tag{11}$$

where  $f$  is the calculated variable,  $V$  is the velocity,  $D$  is the diffusion coefficient,  $Q$  is the source term.

With the finite volume method, equations of type (11) are integrated by the volume of each  $i$ -th cell of the computational grid and by the time interval:

$$\int_{V_i} f dv \Big|_{t=t^{n+1}} - \int_{V_i} f dv \Big|_{t=t^n} + \int_{\tau} \int_{S_i} f V ds dt = \int_{\tau} \int_{S_i} DVf ds dt + \int_{\tau} \int_{V_i} Q dv dt, \tag{12}$$

where  $V_i$  is the volume of the cell,  $S_i$  is the surface of the cell,  $t^n, t^{(n+1)}$  are the time points of the beginning and end of the time step:

$$t^{n+1} = t^n + \tau. \tag{13}$$

When adapting the calculated grid and subgrid geometry resolution, the cell has the shape of an arbitrary polyhedron. Those of the faces that the cell borders with other cells are called "free". The area  $j$  of the free face in the  $i$  cell is denoted by  $S_{ji}$ . "Solid faces" are those faces of a cell that are formed by a border that intersects the cell. The area  $j$  of the solid face in the  $i$  cell is denoted by  $g_i^j$ . Based on these notations, we obtain the expression (12) in the difference form:

$$V_i(f_i^{n+1} - f_i^n) + \sum_j F_i^j S_{ji}^j + \sum_j G_i^j g_i^j + Q_i = 0, \tag{14}$$

where  $Q_i$  is the volume source of the variable  $f$ ,  $f_i^n$  is the averaged value of the variable over the volume of the cell at time  $t^n$ :

$$V_i f_i^n = \int_{V_i} f dv \Big|_{t^n}, \tag{15}$$

the averaged flow densities of the calculated variable  $F_i^j$  and  $G_i^j$  through the corresponding faces  $S_i^j$  and  $g_i^j$  in a time step are determined by the expressions:

$$F_i^j = \int_{\tau} (fV + DVf) dt \Big|_{S_i^j}, \tag{16}$$

$$G_i^j = \int_{\tau} (f_{w_j} V_{w_j} + D(\nabla f)_{w_j}) dt \Big|_{g_i^j}, \tag{17}$$

where the index  $w$  denotes the values of the quantities on the boundary of the computational domain, which corresponds to the face  $g_i^j$ .

The complex  $DVf$  corresponding to the diffusion flow of magnitude  $f$  is approximated in the FlowVision software package by the second order of accuracy in a spatial variable.

One of the most difficult tasks in computer-aided process design is the approximation of the convective flow in the calculated geometry [14–20]. Depending on the required calculation accuracy, several recovery schemes are used (first-order recovery, smooth high-order recovery and stepwise high-order recovery). All these schemes are based on the recovery of the calculated variable  $f$  from its average values inside the cell of the computational grid and the transfer of the recovered liquid along the fluid flow lines. In addition, the so-called «beveled» scheme is used, designed to restore the values in the cells during the diagonal movement of a given medium. It was this scheme that was chosen for further studies of the process of moving the product melt in the forming unit.

This is due to the fact that in the projected area there are areas with a «beveled» direction of movement of the melted product relative to the grid cells. This scheme can be designated as an approximation scheme «with an additional point». It is written in the following form:

$$f(x) = \begin{cases} f_{ri} + f_{xli}(x_{i+1/2} - x), & \text{at } x \geq x_{i+1/2} - 1; \\ f_{li} + f_{xli}(x - x_{i-1/2}), & \text{at } x \leq x_{i+1/2} - 1, \end{cases} \tag{18}$$

where  $l$  is the distance from side  $x_{(i+1/2)}$  to the additional point,  $f_{ri}$  and  $f_{li}$  are the velocity values at the left and right boundaries of the finite volume. Their values are determined from the decomposition of the function into a Taylor series:

$$f(x) = f(x_{i+1/2}) + f'_x \Delta x + \frac{1}{2} f''_{xx} \Delta x^2 + \frac{1}{3!} f'''_{xxx} \Delta x^3 + O(\Delta x^4), \tag{19}$$

where

$$\Delta x = x - x_{i+1/2}. \tag{20}$$

The coefficients of expression (19) are found using definitions of the averaged value of the function of the  $i$ -th finite volume, as well as neighboring  $i-1$  and  $i+1$  volumes.

The result is:

$$f_{ri} = 0.5(f_{i+1} + f_i) - 0.167(f_{i+1} - 2f_i + 2f_{i-1}); \tag{21}$$

$$f_{li} = 0.5(f_i + f_{i-1}) + 0.167(f_{i+1} - 2f_i + 2f_{i-1}).$$

To achieve monotonicity of reconstruction, the values of  $f_{ri}$  and  $f_{li}$  are limited to the average values of neighboring finite volumes:

$$\begin{cases} f_i \leq f_{ri} \leq f_{i+1}, \text{ at } f_{i+1} - f_i \geq 0; \\ f_i > f_{ri} > f_{i+1}, \text{ at } f_{i+1} - f_i < 0; \end{cases}$$

$$\begin{cases} f_{i-1} \leq f_{li} \leq f_i, \text{ at } f_i - f_{i-1} \geq 0; \\ f_{i-1} > f_{li} > f_i, \text{ at } f_i - f_{i-1} < 0. \end{cases} \quad (22)$$

The distance  $l$  and the derivatives  $f_{xri}$  and  $f_{xli}$  on the left and right sides of  $V_i$  are equal:

$$l = \frac{f_i - f_{li}}{f_{ri} - f_{li}}, \quad f_{xri} = \frac{f_{ri} - f_i}{l}, \quad f_{xli} = \frac{f_i - f_{li}}{l-1}. \quad (23)$$

For the numerical solution of the Navier-Stokes equation, we use an implicit splitting algorithm for physical variables. To do this, we write down the equations for the moving volume  $\Omega$ :

$$\int_{V_i} \rho dV = \int_{\Omega_i} \rho dV, \quad (24)$$

$$\int_{V_i} \rho V dV - \int_{\Omega_i} \rho V dV = - \int_{\tau S} P dS dt + D,$$

where  $S$  is the surface of the volume  $\Omega$ ,  $V$  is the velocity field of the specified fluid,  $\rho$  is the density,  $V$  are the terms of the Navier-Stokes equation describing force, gravity, viscous stresses, etc.

The difference analog of the Navier-Stokes equation looks like this:

$$V_i^{n+1} V_i \rho^{n+1} - \int_{\Omega_i} \rho^n V^n dV = -\tau \sum_S P_S^{n+1} s + D_i(V). \quad (25)$$

In this equation, the unknown quantities are  $V^{n+1}$  and  $P^{n+1}$ . Add and subtract additional terms in it as follows

$$\begin{aligned} & (V_i^{n+1} + \bar{V} - \bar{V}) V_i \rho^{n+1} - \int_{\Omega_i} \rho^n V^n dV = \\ & = -\tau \left( \sum_S P_S^{n+1} s - \sum_b P_b^n b + \sum_b P_b^n b \right) + D_i(V). \end{aligned} \quad (26)$$

This equation splits into two:

$$\bar{V} V_i \rho^{n+1} - \int_{\Omega_i} \rho^n V^n dV = -\sum_b P_b^n b + D_i(\bar{V}), \quad (27)$$

and

$$(V_i^{n+1} - \bar{V}) V_i \rho^{n+1} = -\sum_S P_S^{n+1} s + \sum_b P_b^n b. \quad (28)$$

In (27), the pressure field taken at the previous time step is used. This vector equation represents three convective-diffusion transport equations for the three components of the fluid velocity. For further solution, it is split as follows:

$$\hat{V}_i = \frac{1}{V_i \rho^{n+1}} \left( \int_{\Omega_i} V^n dV - \tau \sum_b P_b^n b \right), \quad (29)$$

$$\bar{V}_i = \hat{V}_i + \frac{1}{V_i} D_i(\bar{V}). \quad (30)$$

To determine the pressure field, consider the incompressible fluid condition, from which it can be seen that:

$$\sum_S V_S^{n+1} s = 0, \quad (31)$$

where  $V_S^{n+1}$  is the velocity value at the boundaries of the finite volume  $V_i$ .

To obtain expressions for  $V_S^{n+1}$ , we write down an analog of equation (28) obtained by integrating the Navier-Stokes equations over the moving face of the volume  $\Omega$ . For the face of this volume, which coincides with the face  $b$  at  $t=t_n$  and with at  $t+t_{n+1}$ , the expression for  $V_S^{n+1}$  will have the form:

$$V_S^{n+1} = \bar{V}_S + \frac{\tau}{P_b^{n+1}} \left( \nabla P^{n+1} \right)_b - \frac{\tau}{P_S^{n+1}} \left( \nabla P^{n+1} \right)_S. \quad (32)$$

Substituting the  $V_S^{n+1}$  result into expression (31) we get:

$$\sum_S \frac{\tau}{P_S^{n+1}} \left( \nabla P^{n+1} \right)_S = \sum_S \bar{V}_S s + \sum_b \frac{\tau}{P_b^{n+1}} \left( \nabla P^{n+1} \right)_b. \quad (33)$$

After finding the pressure field  $P^{n+1}$  from (28), the velocity field  $V_S^{n+1}$  is calculated. To prevent fluctuations of the pressure field on non-weighted grids in FlowVision, the difference between the representation of the pressure gradient by the second and fourth order of accuracy is introduced in equation (31). After entering the basic physical parameters and setting the boundary conditions, the computational grid is adapted. After that, the calculation of the matrix channel is started according to the specified conditions.

In order to present a visual picture of the velocity and pressure distribution along the length of the cone-ring forming channel in the FlowVision postprocessor, the computational model was divided into 16 planes perpendicular to the axis of symmetry in 2 mm increments for visual analysis of the complex three-dimensional flow of the melted product. Two layers were created for each plane – velocity and pressure characteristics. During the calculation, the program created a separate file in which the calculation results of each iteration were saved. After the calculation studies are completed, the software package allows you to create a layer with a palette (pressure fill) in the working area of the postprocessor on each calculation plane and display an information window with associated values of the calculated variable. Based on the resulting color scale of the pressure distribution along the length of the cone-ring channel, the dynamics of the process of extrusion of combined feeds were judged (Fig. 4–12).

When processing the received files, graphical dependences of velocity and pressure changes along the length of the cone-ring channel were constructed for various groups of combined feeds with different densities with different angular rotation speeds of the auger with a parallel (Fig. 13), narrowing (Fig. 14) and expanding (Fig. 15) channel between the outer surface of the cone of the auger and the inner surface of the cone of the die.

In the process of designing the forming cone-ring channel, three volumes of changes in the shape geometry of the die were revealed, at the boundaries of the transition of which extremum points are observed.

The pressure in Fig. 4–12 is given in Pascals.

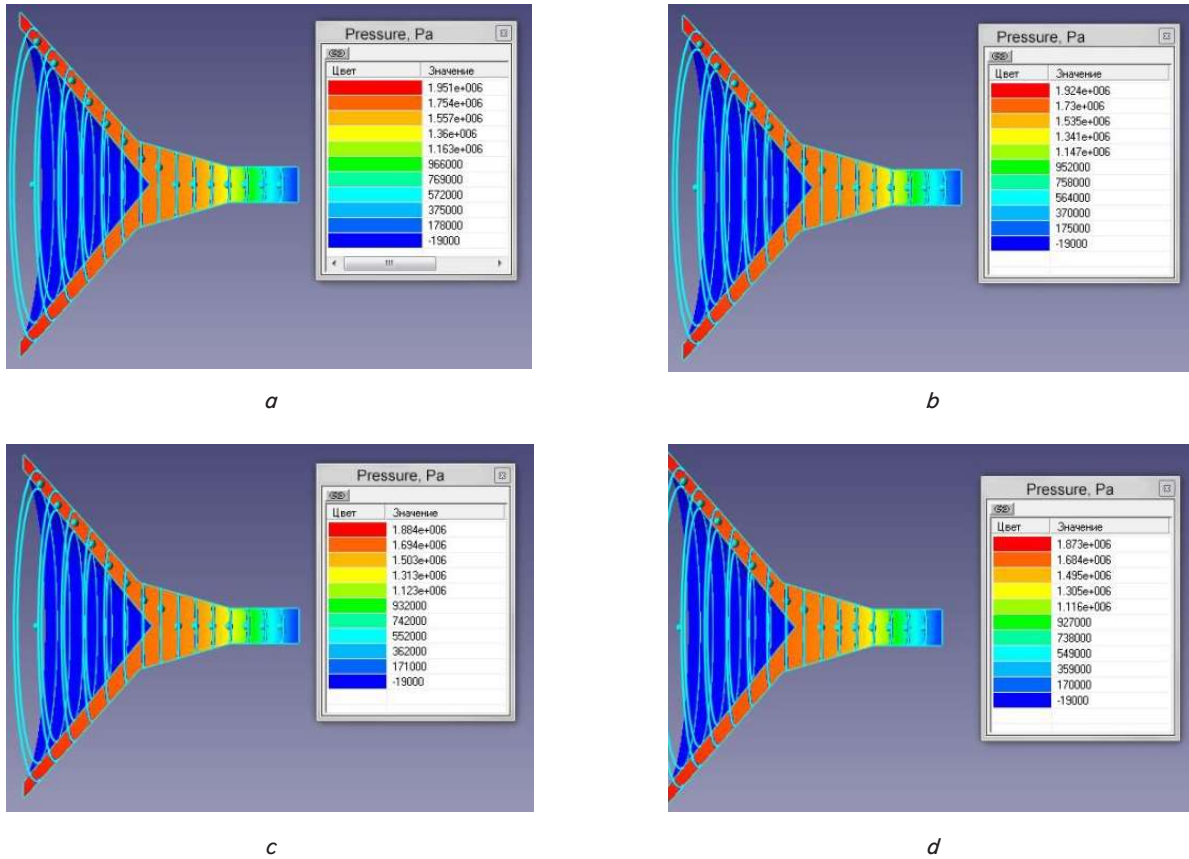


Fig. 4. Change in the pressure of the melt flow of the product with a density of  $1,120 \text{ kg/m}^3$  along the length of the expanding cone-ring channel of the die at the screw rotation speed: *a* –  $20 \text{ rad/s}$ ; *b* –  $30 \text{ rad/s}$ ; *c* –  $40 \text{ rad/s}$ ; *d* –  $50 \text{ rad/s}$

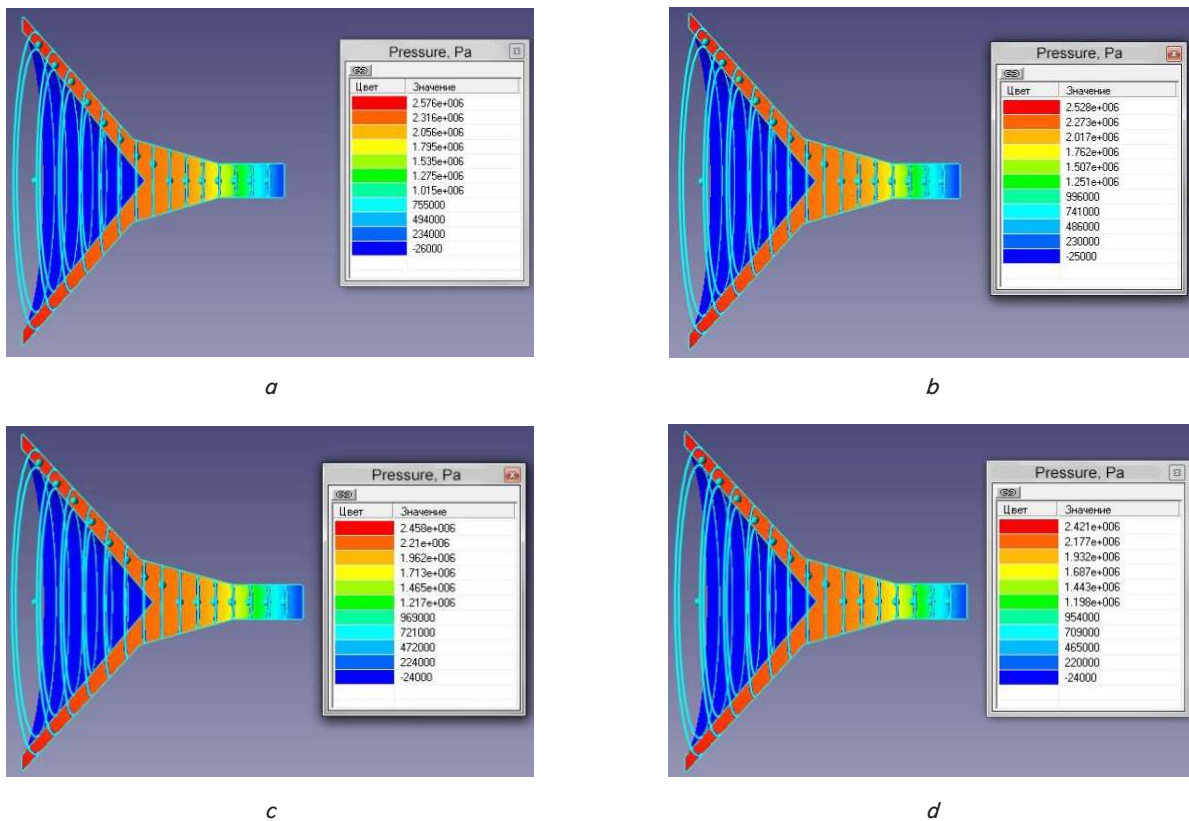


Fig. 5. Change in the pressure of the melt flow of the product with a density of  $1,170 \text{ kg/m}^3$  along the length of the expanding cone-ring channel of the die at the screw rotation speed: *a* –  $20 \text{ rad/s}$ ; *b* –  $30 \text{ rad/s}$ ; *c* –  $40 \text{ rad/s}$ ; *d* –  $50 \text{ rad/s}$

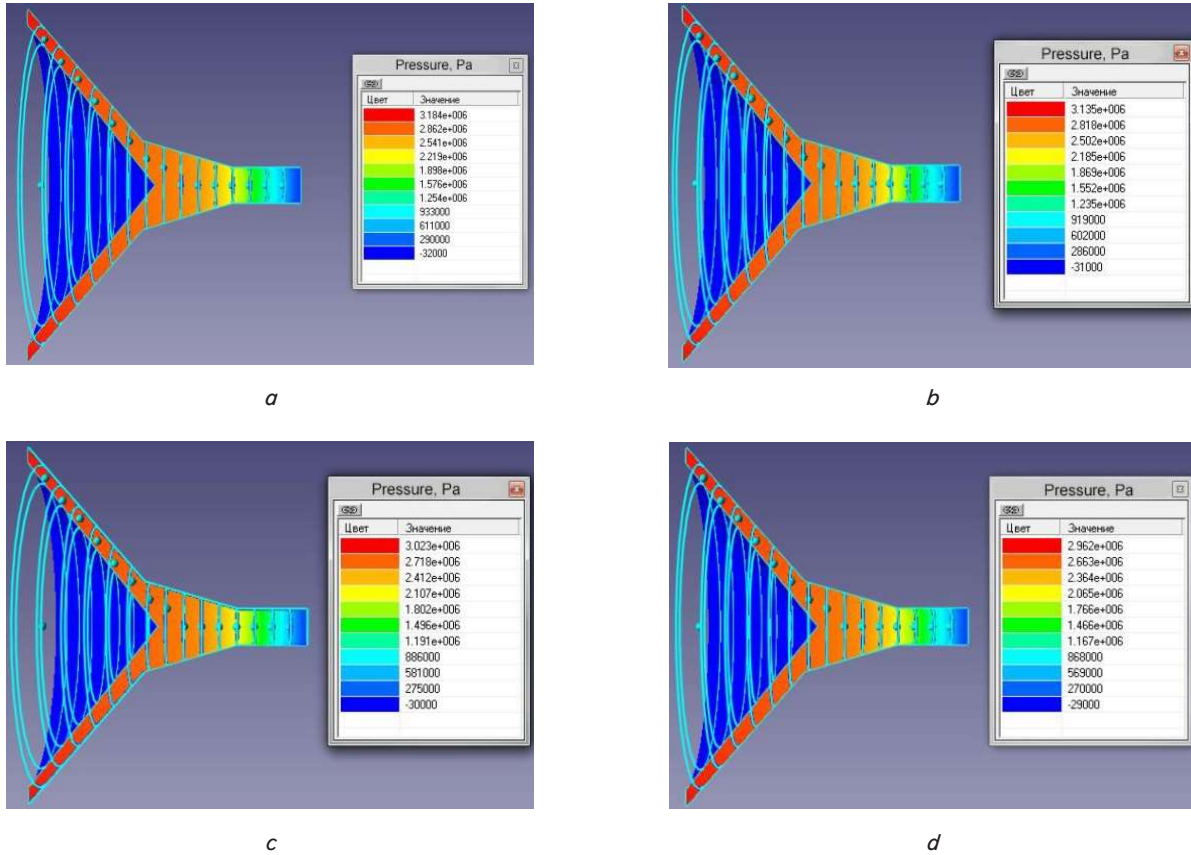


Fig. 6. Change in the pressure of the melt flow of the product with a density of 1,210 kg/m<sup>3</sup> along the length of the expanding cone-ring channel of the die at the screw rotation speed: a – 20 rad/s; b – 30 rad/s; c – 40 rad/s; d – 50 rad/s

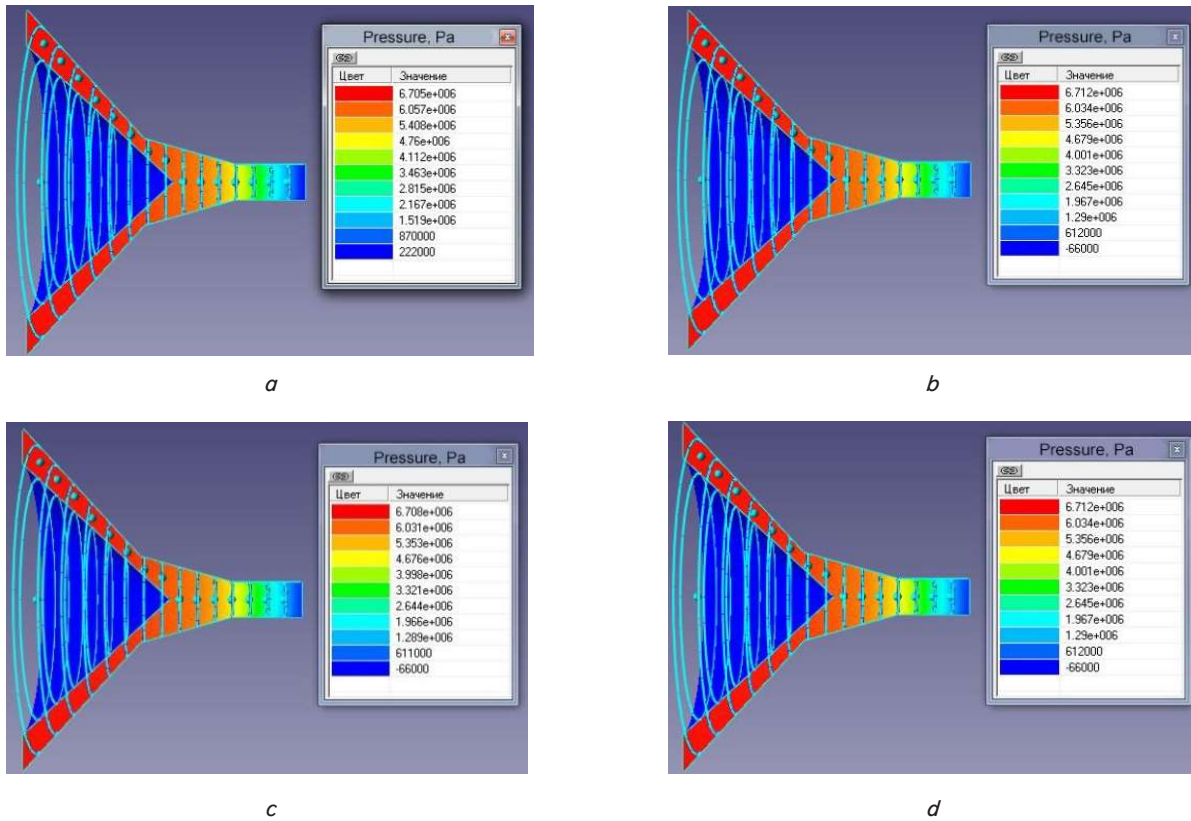


Fig. 7. Change in the pressure of the melt flow of the product with a density of 1,120 kg/m<sup>3</sup> along the length of the tapering cone-ring channel of the die at the screw rotation speed: a – 20 rad/s; b – 30 rad/s; c – 40 rad/s; d – 50 rad/s

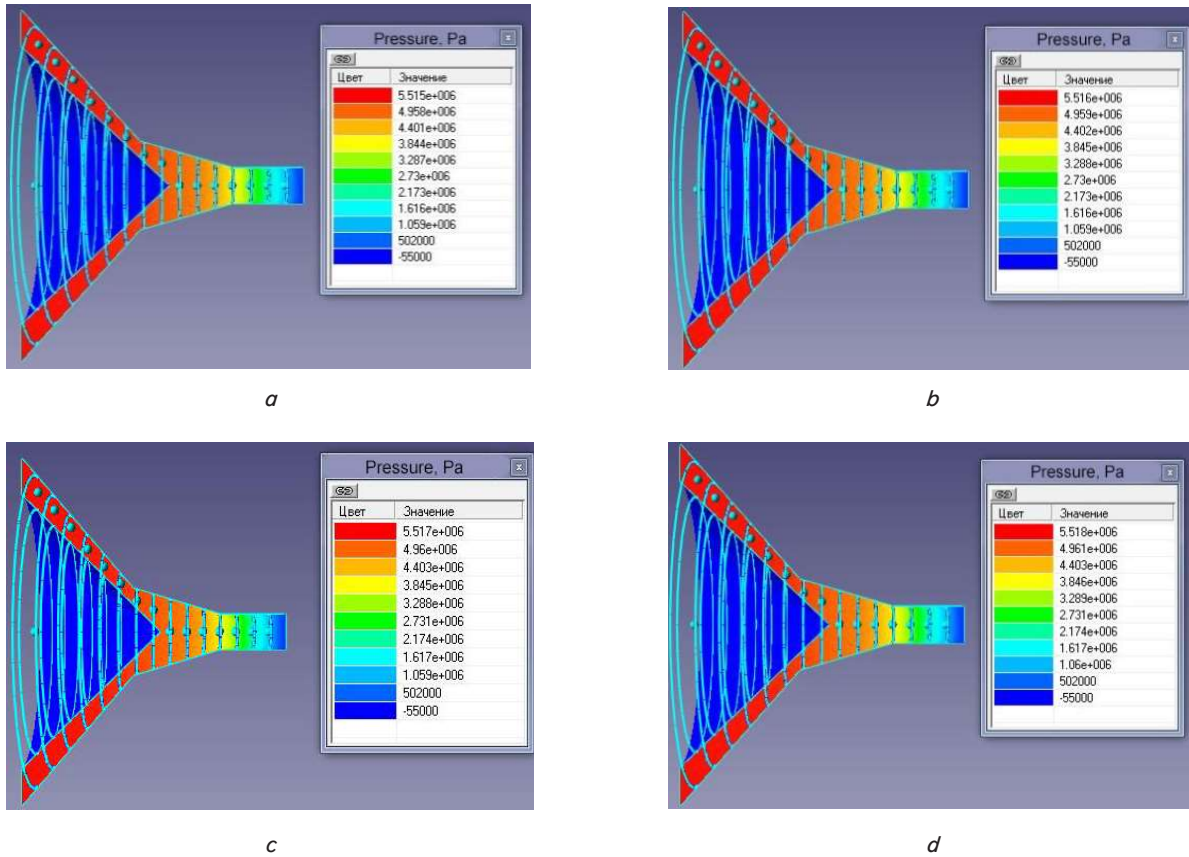


Fig. 8. Change in the pressure of the melt flow of the product with a density of  $1,170 \text{ kg/m}^3$  along the length of the tapering cone-ring channel of the die at the screw rotation speed: *a* – 20 rad/s; *b* – 30 rad/s; *c* – 40 rad/s; *d* – 50 rad/s

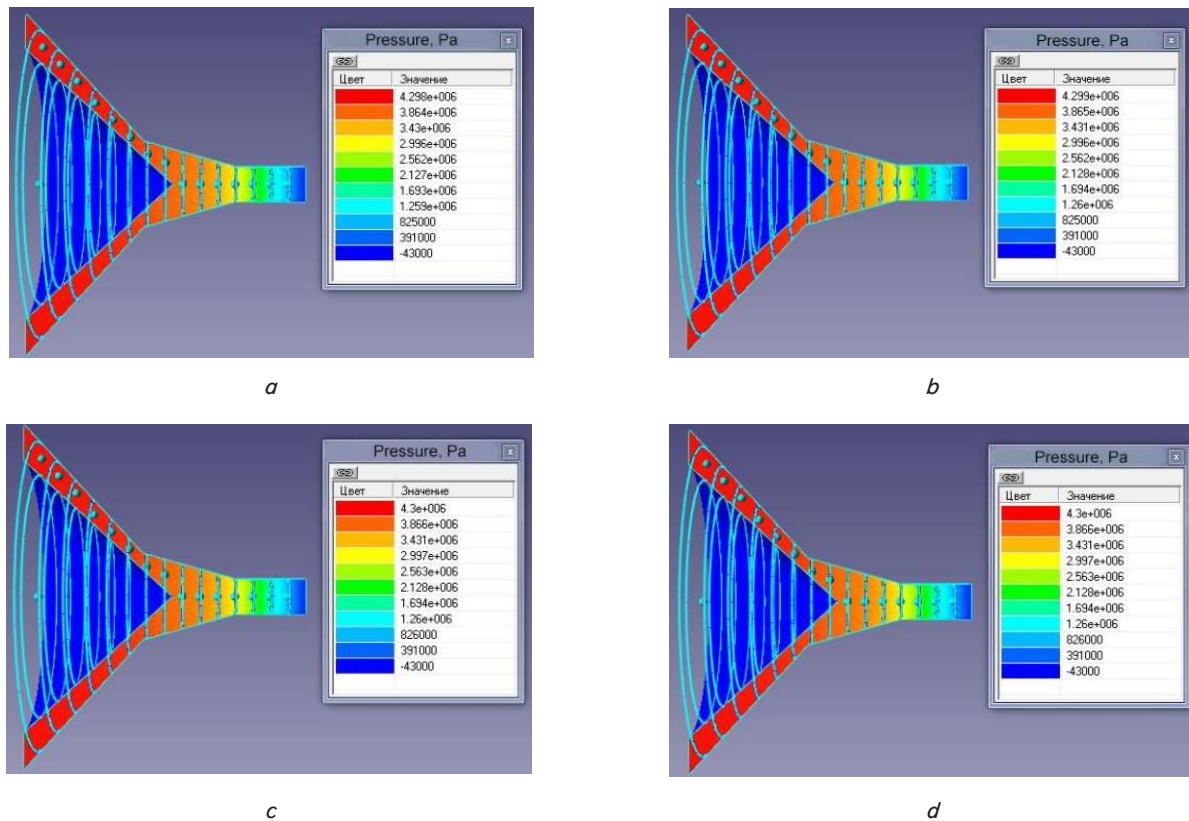


Fig. 9. Change in the pressure of the melt flow of the product with a density of  $1,210 \text{ kg/m}^3$  along the length of the tapering cone-ring channel of the die at the screw rotation speed: *a* – 20 rad/s; *b* – 30 rad/s; *c* – 40 rad/s; *d* – 50 rad/s

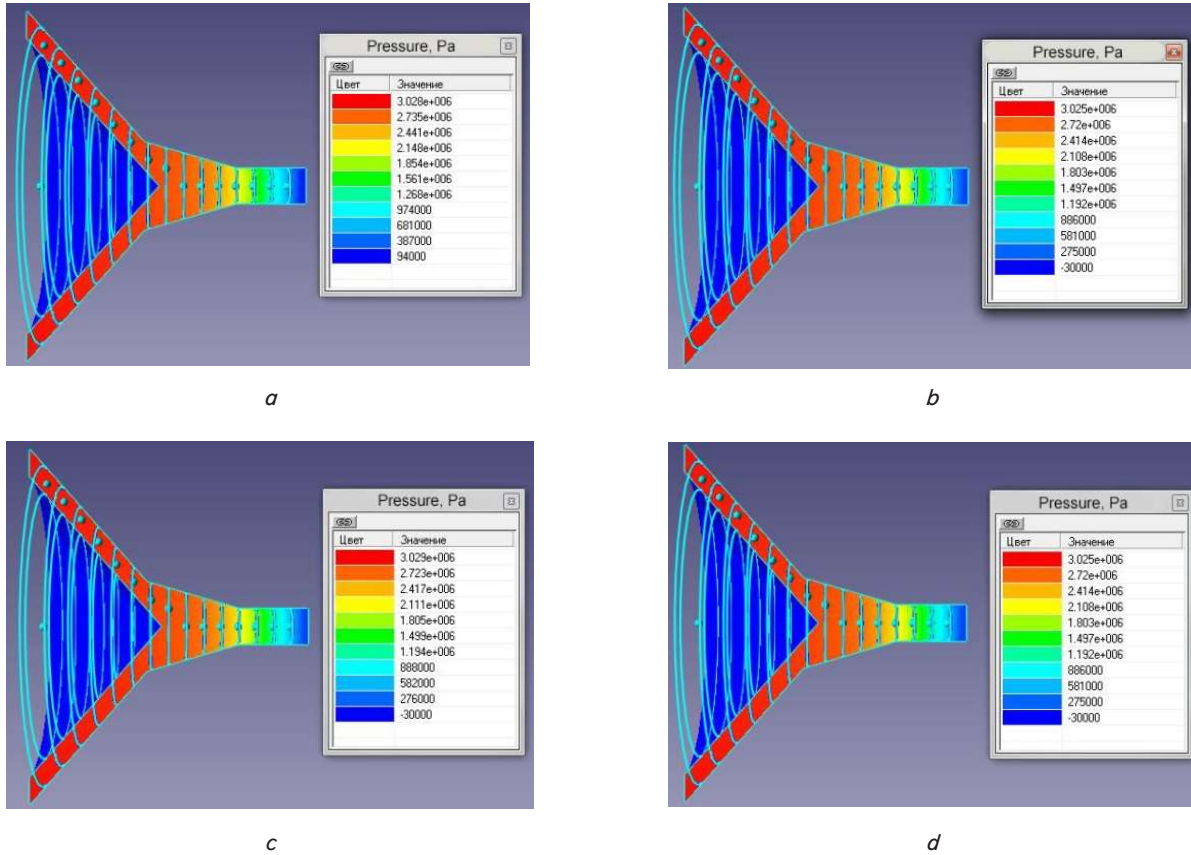


Fig. 10. Change in the pressure of the melt flow of the product with a density of 1,120 kg/m<sup>3</sup> along the length of the parallel cone-ring channel of the die at the screw rotation speed: a – 20 rad/s; b – 30 rad/s; c – 40 rad/s; d – 50 rad/s

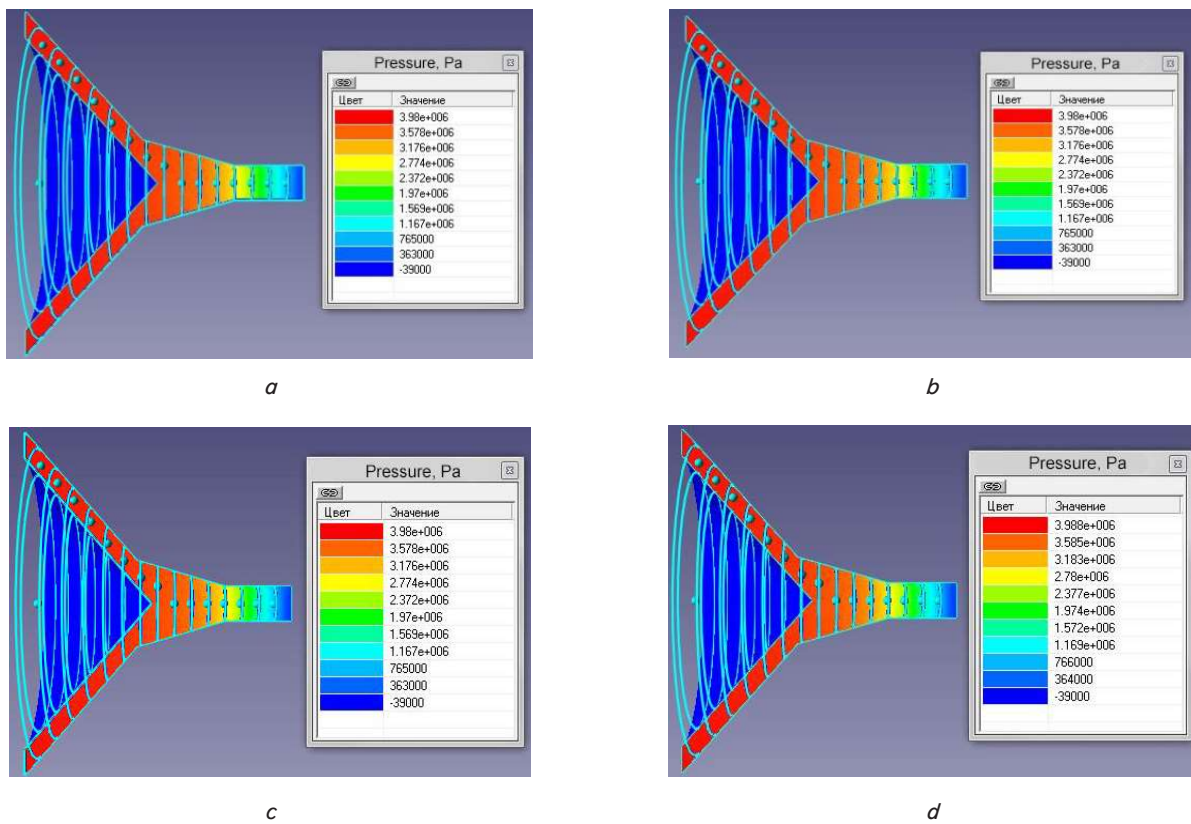


Fig. 11. Change in the pressure of the melt flow of the product with a density of 1,170 kg/m<sup>3</sup> along the length of the parallel cone-ring channel of the die at the screw rotation speed: a – 20 rad/s; b – 30 rad/s; c – 40 rad/s; d – 50 rad/s

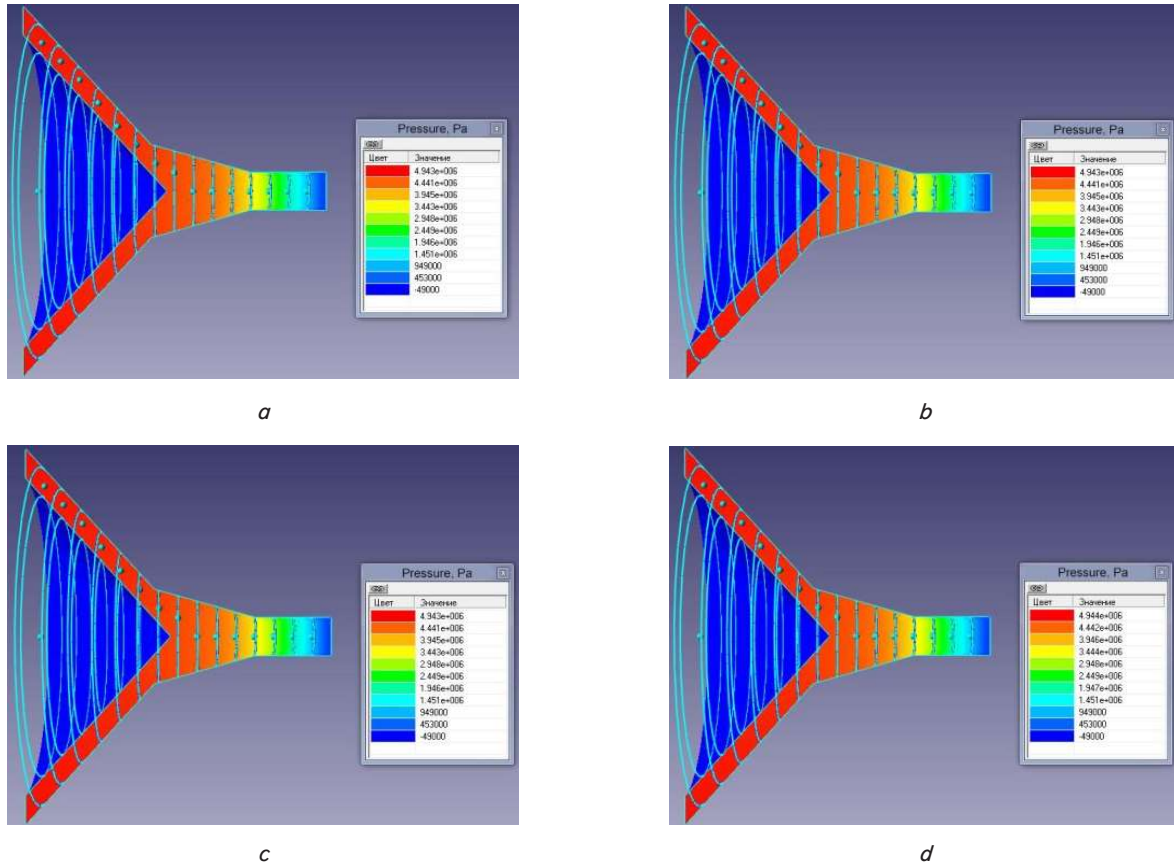


Fig. 12. Change in the pressure of the melt flow of the product by the density of  $1,210 \text{ kg/m}^3$  along the length of the parallel cone-ring channel of the die at the screw rotation speed: *a* – 20 rad/s; *b* – 30 rad/s; *c* – 40 rad/s; *d* – 50 rad/s

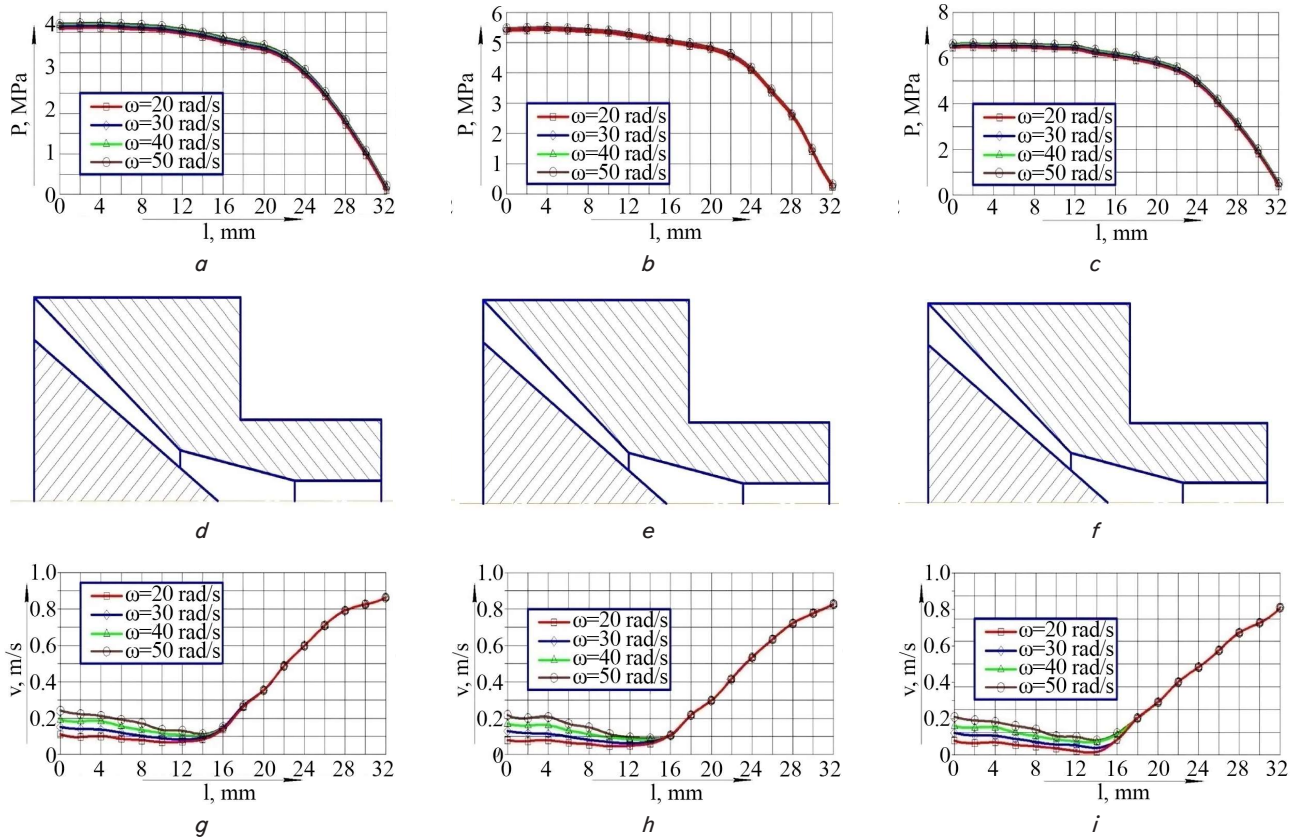


Fig. 13. Graphical dependences of pressure and velocity changes along the length of the tapering forming channel for a product with different densities: *a, d, g* –  $1,120 \text{ kg/m}^3$ ; *b, e, h* –  $1,170 \text{ kg/m}^3$ ; *c, f, i* –  $1,210 \text{ kg/m}^3$

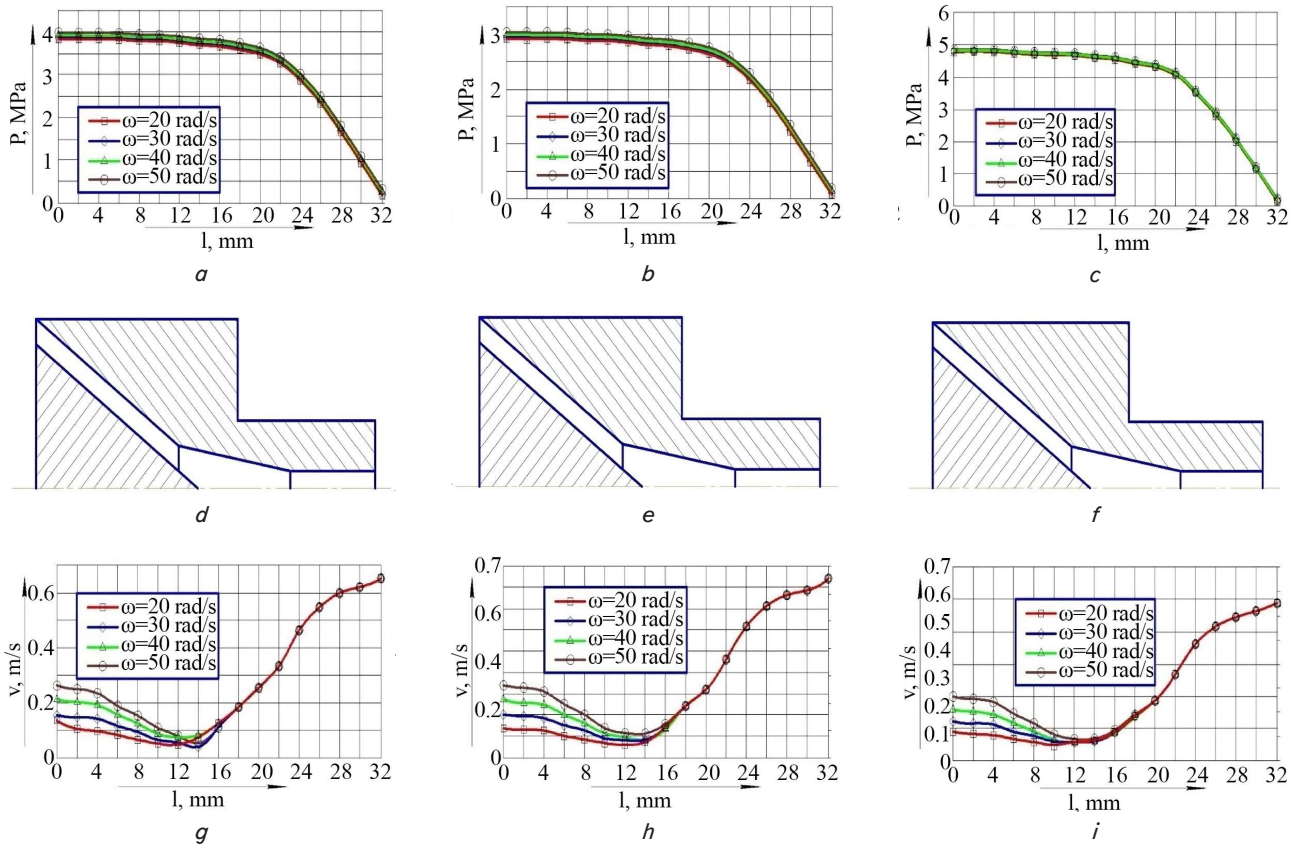


Fig. 14. Graphical dependences of pressure and velocity changes along the length of the parallel forming channel for a product with different densities: *a,d,g* – 1,120 kg/m<sup>3</sup>; *b,e,h* – 1,170 kg/m<sup>3</sup>; *c,f,i* – 1,210 kg/m<sup>3</sup>

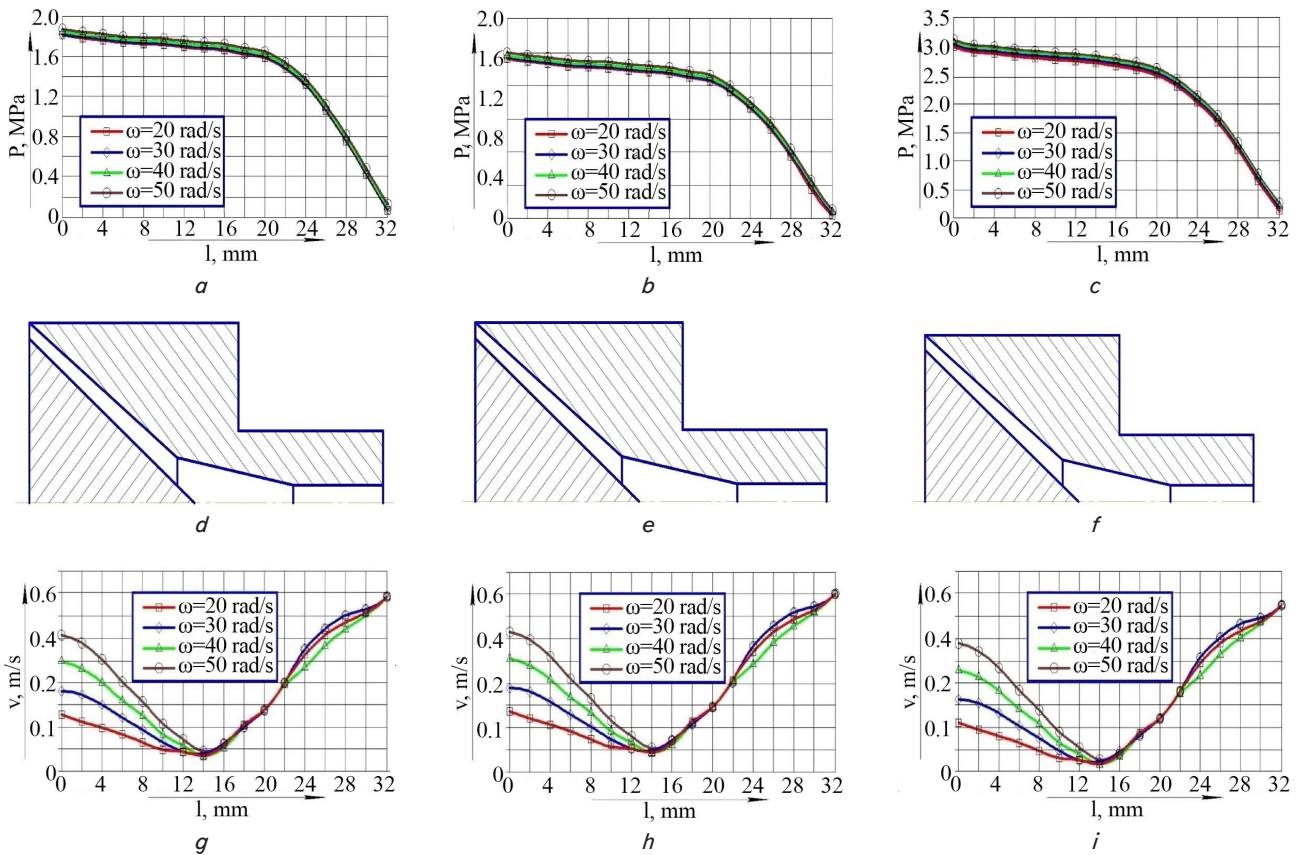


Fig. 15. Graphical dependences of pressure and velocity changes along the length of the expanding forming channel for a product with different densities: *a,d,g* – 1,120 kg/m<sup>3</sup>; *b,e,h* – 1,170 kg/m<sup>3</sup>; *c,f,i* – 1,210 kg/m<sup>3</sup>

The first area is the volume due to the influence of the rotation of the screw and the inner conical surface of the die, the second is a truncated cone of a larger volume, the third is a cylinder. When analyzing the graphical dependence in the narrowing channel in the first area under the influence of the rotating screw, for the first formula of combined feed having a density of  $1,120 \text{ kg/m}^3$ , a slight decrease in pressure within 2.9 % of the pressure at the entrance to the matrix is observed.

For the second formula of combined feed (density  $1,170 \text{ kg/m}^3$ ) and the third (density  $1,210 \text{ kg/m}^3$ ), there was also a decrease in pressure by 2.7 % and 1.5 %, respectively. The nature of the change in the curve of the modulus of the product melt velocity is similar to the pressure curve, but the decrease is more significant and for three formulations lies in the range from 60 to 55 %, which is explained by a decrease in the influence of the rotating cone of the auger, since the product melt flow is reoriented from rotational motion to rectilinear motion.

In the second area, for all three formulations, the pressure continues to decrease in the range from 14.7 % to 15.4 %. At the same time, the velocity modulus in the second volume of the truncated cone begins to increase sharply in the range of 5.3–6.6 times, which is due to a complete reorientation of the direction of movement and a decrease in the cross-sectional area from the base to the top of the truncated cone.

In the third region, there is a further decrease in pressure for all three formulations within 95 % of the pressure value in the previous section before exiting the die.

The velocity modulus in the last section continues to increase smoothly from 45 to 66 % of the velocity value in the previous section before leaving the die. This is due to the transition of the melt from the region of a truncated cone (confuser) to a cylindrical region, where, with a small length of the section, the masses of the product melt randomly move. The laminar flow regime begins to collapse and turn into an undeveloped turbulent regime. The authors found that the laminar mode of motion is restored in the third region.

The deviation between the analytical and experimental values of velocity and pressure varied in the range of 9–12 % and 17–22 %, respectively.

The proposed mathematical model formed the basis of the developed design of a six-zone extruder (Fig. 16).

The extruder consists of an electric motor 1, a reducer 2, a loading hopper 3, a combined auger 4, a nozzle 5 for connection to a vacuum line, a nozzle 6 for entering liquid components, adjusting bolts 7, a matrix 8, an unloading chamber 9 for the extrudate outlet, a device for adjusting the size of the output gap using an adjustment rod 10, an unloading tray 11, working chamber 12 (Fig. 16) [21]. Slots 13 are made in the turns of the screw 4. A combined screw 4 is installed inside the working chamber 12, consisting of six zones: I loading and transportation zone, II pre-sealing zone, III vacuuming zone, IV liquid component injection zone, V homogenization zone and VI pressure stabilization zone.

## 6. Discussion of the results of mathematical modeling and optimization of melt flow of the extruder matrix

The device for adjusting the size of the output gap using the adjusting rod 10 and the unloading tray 11 form the VII unloading zone. Structurally, the combined screw 4 is assembled from separate screw turns, differing in pitch and diameter, and intermediate rings mounted on a smooth shaft and fixed from turning with a key.

In the I zone of loading and transportation, the diameters of the shaft and the screw turns, as well as the pitch of the screw turns are constant. At the end of the I zone of loading and transportation, the screw turn 4 has a gap, in place of which an annular track of constant diameter is made on the screw shaft.

In the II zone of pre-sealing, the screw shaft 4 has a constant, but larger diameter than in the loading and transportation zone. The thickness of the coils is increased, and at the end of the second zone, the screw coil has a gap.

In the III vacuuming zone, the diameter of the screw shaft 4 is made conical (constantly increasing), and in the housing at the beginning of this zone there is a branch pipe 5 for connection to the vacuum line.

In the IV zone of liquid components input, the shaft diameter and the pitch of the turns are constant and, starting from this zone and up to the end of the screw, slots 13 are made in the turns, and in the housing at the beginning of this zone there is a branch pipe 6 for liquid components input.

In the V zone of homogenization, the diameter of the screw shaft 4 is made conical (constantly increasing).

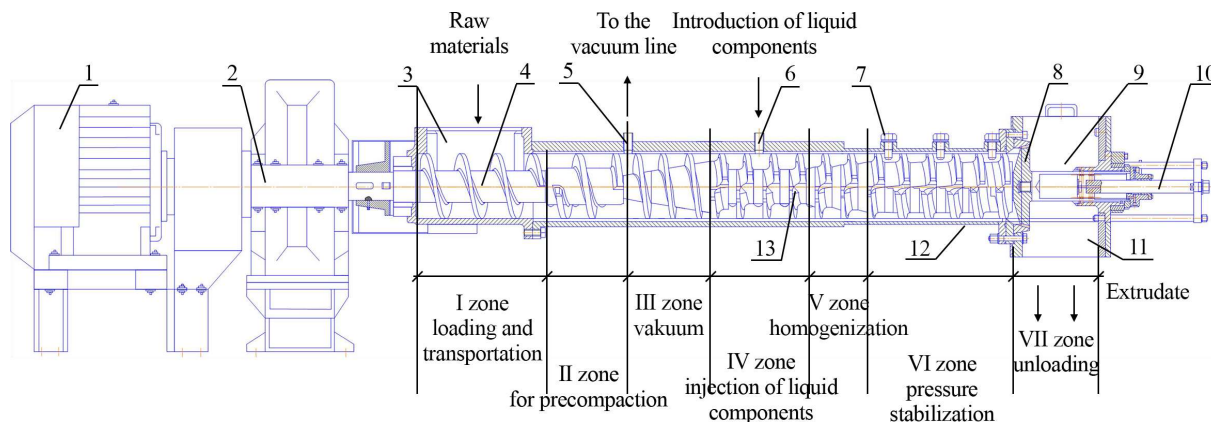


Fig. 16. Extruder: 1 – electric motor; 2 – gearbox; 3 – loading hopper; 4 – combined auger; 5 – pipe for connection with a vacuum line; 6 – pipe for liquid components input; 7 – adjusting bolts; 8 – matrix; 9 – unloading chamber for extrudate outlet; 10 – adjusting rod; 11 – unloading tray; 12 – working chamber; 13 – slots

In the VI pressure stabilization zone, the shaft diameter is constant and has a maximum size, and body length of this zone, with a step equal to the distance between the discontinuities along the axis of the annular lanes is equipped with adjustment screws 7.

The discharge chamber 9 to exit the extrudate is equipped with a device to control the values of the output gap using the adjusting rod 10 using movable in the horizontal plane of the matrix 8.

The unloading chamber 9 is equipped with an unloading tray 11.

Starting from the IV zone and up to the end of the screw, slots 13 are made in the screw turn 4, the presence of which in the screw turns leads to the turbulence of the moving product and reduces the rate of increase in product temperature due to the dissipation effect.

The extruder works as follows (Fig. 16).

The adjustable electric motor 1 is switched on, which, through the gearbox 2, rotates the combined screw 4. The feedstock is fed into the loading hopper 3, from which it enters the I zone of loading and transportation of the working chamber 12. When the screw 4 rotates, the processed product is transported inside the working chamber 12.

Here the product is intensively mixed and moves along the screw 4. Because the diameter of the screw shaft in this zone is constant and the diameter and pitch of the screw turns are also constant, the product is moved along the screw channel of the combined screw 4. At the end of the I zone of loading and transportation, the screw coil has a gap, after which an annular track of constant diameter is made on the screw shaft. The purpose of the screw coil break is that it contributes to additional turbulence of the transported flow when moving the product from the I loading and transportation zone to the II pre-compaction zone. Due to the fact that in zone II the screw shaft 4 has a constant, but larger diameter than in the I zone of loading and transportation and the thickness of the turns is increased, then there is a decrease in the working volume of the inter-turn space along the screw 4. Due to the fact that in this zone the screw shaft has a constant, but larger diameter than in the I zone of loading and transportation, i.e. there is a decrease in the volume of the inter-turn space, then the product begins to condense, displacing air. As a result, the processed product is compacted and compressed. At the same time, using nozzle 5 connected to the vacuum line, a low-pressure area (vacuum) is created in zone III and the air is removed from it. Due to the rupture of the screw coil at the end of zone II and the reduction of the shaft diameter at the beginning of the III evacuation zone, optimal conditions for air removal have been created. Due to the fact that the diameter of the screw shaft 4 in it is made conical (constantly increasing), the product is compressed. As a result of a decrease in the free volume of the turns in the course of the material movement, due to a decrease in the pitch and an increase in the shaft diameter from the beginning to the end of the screw shaft 4, the material is compressed. At the same time, pressure arises in the material. From the III vacuuming zone, the product moves to the IV liquid component input zone, in which the shaft diameter and the pitch of the turns are constant, and slots 13 are made in the turns of the screw 4. At the same time, liquid components are introduced through nozzle 6 located in the housing at the beginning of this zone.

In the future, the product is moved to the V homogenization zone. Due to the fact that in the V zone of homogeni-

zation, the diameter of the screw shaft is conical (constantly increasing), the pressure in it increases, which leads to the melting of small inclusions. The melt is intensively mixed with a screw 4 and turbulates the flow.

In the second stabilization zone, the pressure and temperature fields of the material are re-equalized. The third compression zone allows you to obtain the required final pressure of the product, by reducing the pitch of the screw turns.

When the product is further moved to the VI pressure stabilization zone, due to the fact that the shaft diameter is constant and has a maximum size, pressure stabilization occurs.

The annular tracks of constant diameter made after a rupture on the screw shaft 4 are designed to move the adjusting bolts 7 in the radial direction. Bolts 7, when twisted, enter the inter-turn space VI of the working chamber zone 12, filling the space above the annular track, while the volume of the screw channel decreases, which in turn leads to an increase in the pressure of the displaced flow.

In the turns of the screw 4, slots 13 are made in this zone, between which annular tracks 16 are made on the screw shaft. The product, passing through the slots 13 in the turns of the screw, is turbulated. The adjusting bolts 7 located above the ring tracks, when moving in the radial direction, change the volume of the screw channel, which in turn leads to an increase (when tightening the bolts 7) or a decrease (when unscrewing the bolts 7) of the pressure of the transported product flow.

The extruded material at the outlet of the working chamber 12 meets with a device 10 that regulates the thickness of the output slit using a movable matrix 8. The adjusting device 10 provides pressure regulation in the working chamber 12 of the extruder.

In the VI pressure stabilization zone, a melt homogeneous in structure and temperature is finally formed, the presence of slots in the turns of the screw 4 facilitates the passage of the product and extrusion through the matrix 8.

The geometric dimensions of the slots 13 in the turns of the screw 4 in the IV, V and VI zones, as well as the number, pitch and diameter of the adjustment bolts 7 in the VI pressure stabilization zone, depend on the properties of the processed material and the technological mode of processing.

With the help of the adjusting rod 10, located in the device for regulating the size of the output gap, the required pressure value in the VI zone is adjusted and set.

When exiting the extruder into the unloading chamber 9, as a result of a large pressure drop, the homogeneous mass swells (its explosion occurs). Due to the gelatinization of starch, the destruction of cellulose-lignin formations, its nutritional value is significantly improved.

The finished product is removed from the chamber 9 by the unloading tray 11.

The proposed extruder has the following advantages:

- the extrusion process in it is adapted by the basic kinetic laws of the extrusion process;
- obtaining an extrudate with a given chemical composition is achieved by using an adjustable pressure along the length of the working chamber 12;
- the possibility of improving the quality of the extrudate by vacuuming and introducing liquid thermolabile components and the use of softer, “gentle” temperature regimes and uniform processing;
- extrusion of various raw materials due to a smooth, gradual increase in temperature and pressure with their

stepwise stabilization, necessary for the course of physico-chemical changes in the main components of products;

– universalization of the extruder, i.e. its use in the extrusion of various products of plant or animal origin.

The disadvantages are the governing equations are presented in dimensionless form.

However, the transition from dimensionless quantities to the real (dimensional) geometric characteristics of the screw was obtained as a result of a machine experiment. In particular, on the basis of a single-screw extruder, three forming channels of the matrix were designed to select the most optimal geometric parameters of the die (Fig. 4–12), which affect the depth of physico-chemical transformations occurring in the structure of the combined feeds. When processing the data obtained, graphical dependences of velocity and pressure changes along the length of the cone-ring channel were constructed for various groups of combined feeds with different densities with different angular speeds of screw rotation (Fig. 13–15).

---

## 7. Conclusions

---

1. The optimal geometric shape of the annular gap should be considered a narrowing channel formed by the outer surface of the screw cone and the inner surface of the cone of the die channel, because it is this shape of the channel that makes it possible to change the molecular structure of the product by creating the maximum pressure.

2. The recommended angular rotation speed of the extruder screw is 40–50 rad/s, because it is in this range of values that the deep melting of the product occurs due to the conversion of the mechanical energy of the screw into thermal energy, as well as due to internal friction directly in

the product itself when the extruder is operating in autogenous mode.

The results of mathematical modeling formed the basis for the production of an experimental sample of a die with optimal geometric dimensions, and the conducted series of experiments confirmed the adequacy of the calculations of the mathematical model.

The deviation between the analytical and experimental values of velocity and pressure varied in the range of 9–12 % and 17–22 %, respectively.

---

## Conflicts of interest

---

The authors declare that they have no conflict of interest in relation to this research, whether financial, personal, authorship or otherwise, that could affect the research and its results presented in this paper.

---

## Financing

---

The study was performed without financial support.

---

## Data availability

---

The manuscript has no associated data.

---

## Use of artificial intelligence

---

The authors have used artificial intelligence technologies within acceptable limits to provide their own verified data, which is described in the research methodology section.

---

## References

1. Alimkulov, Zh. S., Veliamov, M. T., Fazylova, K. N., Shaulyeva, K. T., Bektursunova, M. J. (2020). Optimization mathematical models of raw material crushing in the production of compound feeds based on enriching feed concentrate. *Bulletin of the South Ural State University. Ser. Food and Biotechnology*, 8 (2), 29–36.
2. Borovsky, A. Yu., Kizatova, M., Sultanova, M., Abdrakhmanov, H. (2019). Mathematical foundations of the technological process of obtaining combined feeds. *Actual problems of modernity*, 3, 155–159.
3. Enayati, S., Ayoub, A. (2018). Applying Mathematical Optimization To Efficiently Make Better Decisions for Extrusion Technology: State-of-the-Art and Opportunities. *Biomass Extrusion and Reaction Technologies: Principles to Practices and Future Potential*, 243–260. <https://doi.org/10.1021/bk-2018-1304.ch013>
4. Malik, M., Kalyon, D. M., Golba, J. C. (2014). Simulation of Co-Rotating Twin Screw Extrusion Process Subject to Pressure-Dependent Wall Slip at Barrel and Screw Surfaces: 3D FEM Analysis for Combinations of Forward- and Reverse-Conveying Screw Elements. *International Polymer Processing*, 29 (1), 51–62. <https://doi.org/10.3139/217.2802>
5. Wu, K., Sun, Y., Peng, B., Ding, W., Wang, S. (2013). Modeling and experiment on rotary extrusion torque in ring-die pelleting process. *Nongye Gongcheng Xuebao/Transactions of the Chinese Society of Agricultural Engineering*, 29 (24), 33–39. <https://doi.org/10.3969/j.issn.1002-6819.2013.24.005>
6. Chaturvedi, E., Rajput, N. S., Upadhyaya, S., Pandey, P. K. (2017). Experimental Study and Mathematical Modeling for Extrusion using High Density Polyethylene. *Materials Today: Proceedings*, 4 (2), 1670–1676. <https://doi.org/10.1016/j.matpr.2017.02.006>
7. Nahemiah, D. (2016). Application of Response Surface Methodology (RSM) for the Production and Optimization of Extruded Instant Porridge from Broken Rice Fractions Blended with Cowpea. *International Journal of Nutrition and Food Sciences*, 5 (2), 105. <https://doi.org/10.11648/j.ijnfs.20160502.13>
8. Atukuri, J., Odong, B. B., Muyonga, J. H. (2019). Multi response optimization of extrusion conditions of grain amaranth flour by response surface methodology. *Food Science & Nutrition*, 7 (12), 4147–4162. <https://doi.org/10.1002/fsn3.1284>
9. Kizatova, M. Y., Sultanova, M. Zh., Borovsky, A. Y., Muslimov, N. Zh., Nokusheva, Z. A., Aitzhanov, Y. S. (2020). Mathematical planning of a multi-factor experiment and optimization of the feed extrusion process. *IOP Conference Series: Materials Science and Engineering*, 994, 012022. <https://doi.org/10.1088/1757-899x/994/1/012022>

10. Schittny, A., Ogawa, H., Huwyler, J., Puchkov, M. (2018). A combined mathematical model linking the formation of amorphous solid dispersions with hot-melt-extrusion process parameters. *European Journal of Pharmaceutics and Biopharmaceutics*, 132, 127–145. <https://doi.org/10.1016/j.ejpb.2018.09.011>
11. Ostrikov, A., Ospanov, A., Vasilenko, V., Muslimov, N., Timurbekova, A., Jumabekova, G. (2019). Melt flow of biopolymer through the cavities of an extruder die: Mathematical modelling. *Mathematical Biosciences and Engineering*, 16 (4), 2875–2905. <https://doi.org/10.3934/mbe.2019142>
12. Adekola, K. A. (2016). Engineering Review Food Extrusion Technology and Its Applications. *Journal of Food Science and Engineering*, 6 (3). <https://doi.org/10.17265/2159-5828/2016.03.005>
13. Mushtruk, M., Gudzenko, M., Palamarchuk, I., Vasylyv, V., Slobodyanyuk, N., Kuts, A. et al. (2020). Mathematical modeling of the oil extrusion process with pre-grinding of raw materials in a twin-screw extruder. *Potravinarstvo Slovak Journal of Food Sciences*, 14, 937–944. <https://doi.org/10.5219/1436>
14. Kushnir, V., Gavrilov, N., Kim, S. (2017). Experimental Studies on Grain Material Extruding Process. *Procedia Engineering*, 206, 1611–1617. <https://doi.org/10.1016/j.proeng.2017.10.686>
15. Lela, B., Musa, A., Zovko, O. (2014). Model-based controlling of extrusion process. *The International Journal of Advanced Manufacturing Technology*, 74 (9-12), 1267–1273. <https://doi.org/10.1007/s00170-014-6054-6>
16. Gomes, K. S., Berwian, G. F., Batistella, V. M. C., Bender, L. E., Reinehr, C. O., Colla, L. M. (2022). Nutritional and Technological Aspects of the Production of Proteic Extruded Snacks Added of Novel Raw Materials. *Food and Bioprocess Technology*, 16 (2), 247–267. <https://doi.org/10.1007/s11947-022-02887-0>
17. Xu, M., Zhang, X., Zhang, Y., Wang, J., Li, J., Hu, Y. et al. (2023). Effect of screw speed, temperature and moisture on physicochemical properties of corn gluten meal extrudate. *Journal of the Science of Food and Agriculture*, 103 (12), 5782–5790. <https://doi.org/10.1002/jsfa.12649>
18. Okunola, A. A., Dottie, E. P., Moses, O. I., Adekanye, T. A., Okonkwo, C. E., Kaveh, M. et al. (2023). Development and Process Optimization of a Ready-to-Eat Snack from Rice-Cowpea Composite by a Twin Extruder. *Processes*, 11 (7), 2159. <https://doi.org/10.3390/pr11072159>
19. Altan, A., Yağci, S. (2023). Physicochemical characteristics and structural changes of fermented faba bean extrudates prepared by twin-screw extrusion. *Food Chemistry*, 411, 135502. <https://doi.org/10.1016/j.foodchem.2023.135502>
20. Bachurina, M., Kazakov, A., Trufanova, N. (2014). Mathematical modelling of stratified flow of polymer melts in an axisymmetric formulation. *PNRPU Mechanics Bulletin*, 2, 102–124. <https://doi.org/10.15593/perm.mech/2014.2.05>
21. Ostrikov, A. N., Afanasiev, V. A., Frolova, L. N., Nesterov, D. A., Sizikov, K. A. (2021). Pat. RF No. 2750158. Extruder.